

The X–ray Spectrum of Cyg X–2

C. Done¹, P. T. Życki² and D. A. Smith³

¹*Department of Physics, University of Durham, South Road, Durham, DH1 3LE, UK*

²*N. Copernicus Astronomical Center, Bartycka 18, 00-716, Warsaw, Poland*

³*University of Maryland, College Park, Maryland, MD20742, USA*

24 October 2018

ABSTRACT

The spectra of disc accreting neutron stars generally show complex curvature, and individual components from the disc, boundary layer and neutron star surface cannot be uniquely identified. Here we show that much of the confusion over the spectral form derives from inadequate approximations for comptonization and for the iron line. There is an intrinsic low energy cutoff in comptonised spectra at the seed photon energy. It is very important to model this correctly in neutron star systems as these have expected seed photon temperatures (from either the neutron star surface, inner disc or self–absorbed cyclotron) of ≈ 1 keV, clearly within the observed X–ray energy band. There is also reflected continuum emission which must accompany the observed iron line, which distorts the higher energy spectrum. We illustrate these points by a reanalysis of the *GINGA* spectra of Cyg X–2 at all points along its Z track, and show that the spectrum can be well fit by models in which the low energy spectrum is dominated by the disc, while the higher energy spectrum is dominated by comptonised emission from the boundary layer, together with its reflected spectrum from a relativistically smeared, ionised disc.

Key words: accretion, accretion discs, radiation mechanisms:thermal, binaries: close, stars: individual: Cyg X-2, stars: neutron, X-rays: stars

1 INTRODUCTION

Disc accreting neutron star systems are amongst some of the brightest X–ray sources in the sky. They can be split into two broad types namely atolls and Z sources (Hasinger & Van der Klis 1989). Observationally these differ in that they show distinct types of spectral variability and timing behaviour, which link more fundamentally to a difference in the accretion rate and probably also in magnetic field (Hasinger & Van der Klis 1989). The atolls have an accretion rate which is typically below $\sim 10\%$ of the Eddington limit, and have weak magnetic fields while the Z sources accrete at 50–150 % of Eddington, and probably have stronger magnetic fields (e.g. the review by Van der Klis 1995). Both types generally show 2–20 keV spectra which exhibit pronounced curvature, probably due to Compton scattering of seed photons by electrons with temperature $kT_e \sim 5$ keV (e.g. White, Stella & Parmar 1988), except at low luminosity states which are only seen in the atoll systems, where the spectrum makes a transition to a power law (e.g. Mitsuda et al., 1989; van Paradijs & van der Klis 1994; Barret et al., 2000).

Here we concentrate on the X–ray spectra of the Z

sources. A full description of the accretion flow for these sources should take into account the interaction of the disc with the stellar surface, including the effects of radiation pressure and magnetic field in a relativistic potential. This is likely to be extremely complex, as shown by initial hydrodynamic (Popham & Sunyaev 2001; Inogamov & Sunyaev 1999) and magnetohydrodynamic simulations (Miller & Stone 1997). The boundary layer/inner disc emission can then illuminate the rest of the disc giving rise to a Compton reflected spectrum and associated iron $K\alpha$ line from the heated, ionised, upper layer of the disc (see e.g. the review by Fabian et al., 2000, with specific application to Z sources by Brandt & Matt 1994). Given this complexity it is perhaps unsurprising that the observed spectra from Z sources (and atolls) have proved difficult to fit (e.g. Mitsuda et al. 1984; White, Stella & Parmar 1988). This led to the widespread use of colour–colour diagrams as opposed to true spectral fitting. Here we show that previous difficulties were mainly caused by using poor approximations for the comptonised and reflected emission components. We include relativistic smearing (Fabian et al., 1989) of the disc emission as the source of the line broadening (which is otherwise very dif-

ficult to explain) and derive excellent fits to the GINGA spectra of Cyg X-2 at all points on its Z track.

2 X-RAY EMISSION MODELS

X-rays can arise from a variety of processes from accretion onto a low magnetic field neutron star. There can be components from the neutron star surface, the boundary layer and the X-ray illuminated disc, and these should be subject to general and special relativistic effects. The thermal emission from the neutron star surface is probably buried beneath a very optically thick boundary layer at the high mass accretion rates seen in the Z sources (Popham & Sunyaev 2001), leaving only the disc and boundary layer as the major emission components. The energy release in the boundary layer heats the material, which then cools predominantly by comptonization of any seed photons. The seed photons can either be from the disc, or from the neutron star surface, or from self-absorbed cyclo/synchrotron photons from the magnetic field (Lamb 1989; Psaltis, Lamb & Miller 1995 but see Wardzinski & Zdziarski 1999). The resulting spectrum is then either clearly comptonised, or quasi-blackbody if the optical depth is large enough to mostly thermalise the emission (saturated comptonization). Further Compton scattering, including bulk motion effects, can take place if the accreting material has a substantial scale height, so that the emission from the boundary layer has to travel through this infalling material before it can escape to the observer (Lamb 1989; Psaltis et al., 1995).

The boundary layer can directly illuminate some fraction of the disc. Part of the illuminating flux is reflected (Smale et al 1993; Brandt & Matt 1994), while the rest is thermalised, enhancing the disc emission (e.g. Czerny, Czerny & Grindley 1986). This heats the upper layers of the disc to the Compton temperature of around 1–2 keV. This exceeds the virial temperature at distances $\geq 3-6 \times 10^{10}$ cm for a $1.4M_{\odot}$ neutron star, so the material escapes as a wind forming a corona around the outer accretion disc (Begelman, McKee & Shields 1983). This accretion disc corona (ADC) is especially important in determining the observational appearance of the highly inclined systems, where the intrinsic, central source is hidden by the disc but can be seen via scattering in this tenuous material above and below the disc (e.g. White, Nagase & Parmar 1995). The photo-ionised ADC emits line and continuum radiation, and can also scatter some of the boundary layer/inner disc emission back onto the disc, increasing the illumination (e.g. Vrtilik, Soker & Raymond 1993). Even at somewhat smaller radii the X-ray illumination heats the upper layers of the discs, so it has an appreciably larger scale height than an unilluminated disc, although the stronger gravity means that it cannot escape to form a wind. The emission from this photo-ionised, heated layer consists of recombination features (line and continuum radiation) together with the reflection of some fraction of the incident X-rays from the disc (Kallman & White 1989; Vrtilik, Soker & Raymond 1993; Ko & Kallman 1994).

3 SPECTRAL MODEL

From the discussion above, the spectrum should consist of components from the disc and boundary layer, together with reflection from the disc and scattering/emission/absorption from the ADC. Generally progress is made by estimating which components dominate so as to form a simplified model which nonetheless describes most of the physical processes. This is where the problems arise as there is no consensus on which effects dominate.

One approach to modelling the spectra (generally called the ‘Eastern model’ in the literature) assumes that an optically thick disc dominates at low energies, while a Comptonised boundary layer dominates at higher energies. This was developed by Mitsuda et al., (1984; 1989), and fits the data well with the addition of a *broad* iron $K\alpha$ line (White, Peacock & Taylor 1985; Hirano et al., 1987; Asai et al., 2000).

However, spectral fitting is inherently non-unique, and another approach is to assume that the majority of the emission at both high and low energies comes from a comptonised disc, while the boundary layer emits as a quasi-blackbody in the middle of this energy range (White et al., 1988). Such models (generally termed ‘Western’ models) can fit the data equally well, but again require the inclusion of a broad iron line component (White et al., 1988; Mitsuda et al., 1989; Hasinger et al., 1990).

Here, we follow the Eastern approach, as it seems most likely that the boundary layer is strongly Comptonised (Popham & Sunyaev 2001). We assume that the low energy X-ray continuum is dominated by the disc, but the disc spectrum is not well known especially at accretion rates close to Eddington where radiation pressure must be important. The radial temperature distribution depends on whether the viscosity is proportional to the gas pressure or the total (gas plus radiation) pressure (Stella & Rosner 1984). Electron scattering in the atmosphere is also expected to be important, leading to weak Comptonization of the disc emission (Shakura & Sunyaev 1973), and the intrinsic disc spectrum should be further broadened by relativistic effects (Ebisawa et al., 1991). Detailed calculations of these distortions show that with a restricted bandpass, where only the high energy tail of the disc spectrum is seen, then the shape of the spectrum can be well approximated by a simple multi-colour disc model with a colour temperature correction (Ebisawa et al., 1991; Shimura & Takahara 1995; Merloni et al. 2000). Thus we approximate the disc spectrum by the `diskbb` model in XSPEC, but also test that this assumption does not strongly bias our results by using other disc spectral models.

We assume that the seed photons for the comptonization in the boundary layer come from the neutron star surface as well as the inner disc, so they can be at higher energies than the observed disc emission. The typical temperatures expected from close to the neutron star at high mass accretion rates are ≈ 1 keV, i.e. within the observed X-ray bandpass. Simple analytic approximations (e.g. the `compst` model or a cutoff power law) for the Compton scattered spectrum are only valid where the seed photon energy is very much lower than that of the hot electrons (e.g. Hua & Titarchuk 1995). Explicit seed photon comptonization models are required (such as the `comptt` model in XSPEC), and these give spectra with significantly different curvature close

to the seed photon energies. Such models are starting to be used to fit broad band (generally SAX) data from Z and atoll systems (Guainazzi et al., 1998; Piraino et al 1999; in't Zand et al., 1999; di Salvo et al., 2000; 2001). However, the assumption in `comptt` is that the seed photons have a Wien distribution. Here instead we assume that the seed photons have a blackbody distribution and use an analytic approximation to the Comptonisation based on the solution of Kompaneets equation (Zdziarski, Johnson & Magdziarz 1996), as described in Życki, Done & Smith (1999).

This comptonising cloud around the neutron star can illuminate the accretion disc, ionising it and producing a characteristic reflected component and iron $K\alpha$ line. This was first detected in Active Galactic Nuclei, and extensively studied both in supermassive and in Galactic Black Holes (see e.g. Fabian et al., 2000 and references therein). However, its application to spectra from neutron star systems is much less widespread. The atoll systems at low mass accretion rate have power law spectra in the 2–20 keV range, and reflection is sometimes included to fit these data (Yoshida et al., 1993; Piraino et al 1999; Barret et al., 2000). However, the curving spectra from higher accretion rate atolls and Z sources have not been fit with reflection models despite observational (Smale et al., 1993) and theoretical (Brandt & Matt 1994) motivation.

Another issue of importance in modelling the reflected spectrum is relativistic smearing. The disc extends down close to the surface of the neutron star, so reflection from the *inner* disc with relativistic distortions on both the line and reflected continuum should be important (Fabian et al 1989). This has been seen in AGN (Tanaka et al., 1995) and Galactic Black Hole Candidates (Życki, Done & Smith 1997; 1998; 1999; Done & Życki 1999) but again has not been studied in high mass accretion rate neutron star systems. Instead the observed strong broad line at 6–7 keV (White et al., 1985; Hirano et al., 1987; Asai et al. 2000) is generally interpreted as arising from the ADC and illuminated *outer* disc (Kallman & White 1989; Raymond 1993), although it is very difficult to make both the observed line intensity and width from such a corona (see e.g. the discussion in Smale et al., 1993).

We calculate the reflected emission from the `thcomp` continuum as described in Życki et al., (1999). This calculates the self consistent line emission as well as the angle dependent reflected continuum for any ionization state and iron abundance (all the other elements are assumed to have solar abundance: Morrison & McCammon 1983). Relativistic smearing (including light bending) is then applied to this total (line plus continuum) spectrum (Fabian et al., 1989). The resultant spectrum depends on the inclination, which we fix at 60° (Orosz & Kuulkers 1999).

We assume that emission/absorption/scattering from the ADC above the outer disc is negligible. This is probably not the case for the low energy spectrum, as line emission is seen at ~ 1 keV in several LMXB's (e.g. Bautista et al., 1998 and references therein) including Cyg X-2 (Kuulkers et al., 1997). However, here we are concerned with the 2–20 keV spectrum, and the iron K line associated with the ADC is probably small as the K/L line ratio is low for the steep spectra characteristic of the Z sources (Kallman 1995).

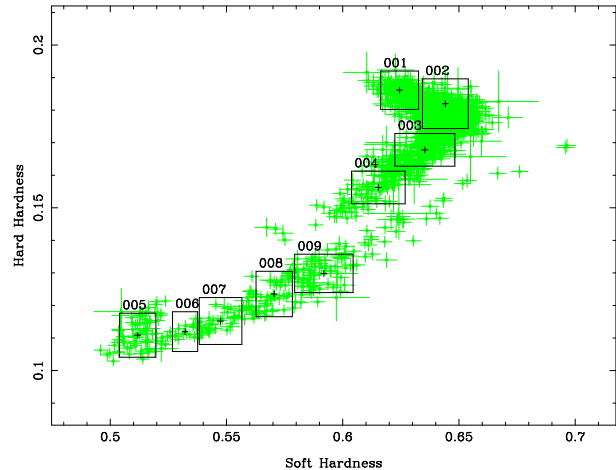


Figure 1. A colour – colour plot showing the Z track of Cyg X-2 in the June 1988 data. The overlaid boxes show the data used to make the individual spectra

Table 1. GINGA observations of Cyg X-2 in June 1988

UT Start	UT End
88-Jun-10 12:35:00	88-Jun-11 05:25:54
88-Jun-11 13:30:00	88-Jun-12 22:30:26
88-Jun-13 13:15:00	88-Jun-14 04:00:34

4 OBSERVATIONS

4.1 GINGA data

We use the Cyg X-2 *Ginga* data, re-extracting them from the original FRF's using the *Ginga* data reduction software at Leicester. Observations were performed in MPC2, MPC3 and PC modes (see Hasinger et al., 1990); however, in this paper, we use only the MPC2 mode data in order to perform a detailed spectral analysis. Data were rejected from periods when the SUD rate (*i.e.* the LAC count rate above 24 keV) exceeded 8 counts/sec/detector, the magnetic cut-off rigidity was outside the range 7–20 GeV/c, the angle between the LAC pointing direction and the Earth's horizon was outside the range 6–120 degrees, and the SOL2 rate (of the solid-state electron detector on board *Ginga*). Unfortunately, the intensity of Cyg X-2 during the observations was such that the register storing the detected count rate overflowed occasionally before telemetry. This affected only data accumulated at medium bit-rate, and could be corrected after examining each PHA spectra. The data were corrected for deadtime using the following formulae:

$$\lambda = \frac{\mu}{1 - \mu_{\text{DET}} \times \tau}, \quad \sigma_{\lambda}^2 = \frac{\sigma_{\mu}^2}{(1 - \mu_{\text{DET}} \times \tau)^2}$$

where, λ and σ_{λ}^2 are the true count rate and variance, μ and σ_{μ}^2 are the observed count rate and variance, μ_{DET} is the observed count rate for one detector integrated over all PHA channels, and τ is the deadtime ($= 1.8 \times 10^{-4}$ seconds). Background subtraction was performed using off-source data taken in a contemporary 3–4 month period, and correcting for the 37-day periodicity of the *Ginga* orbit (*i.e.* the “universal” method of Hayashida et al., 1989; Williams et al., 1992). The spectrum of Cyg X-2 is sufficiently soft as to

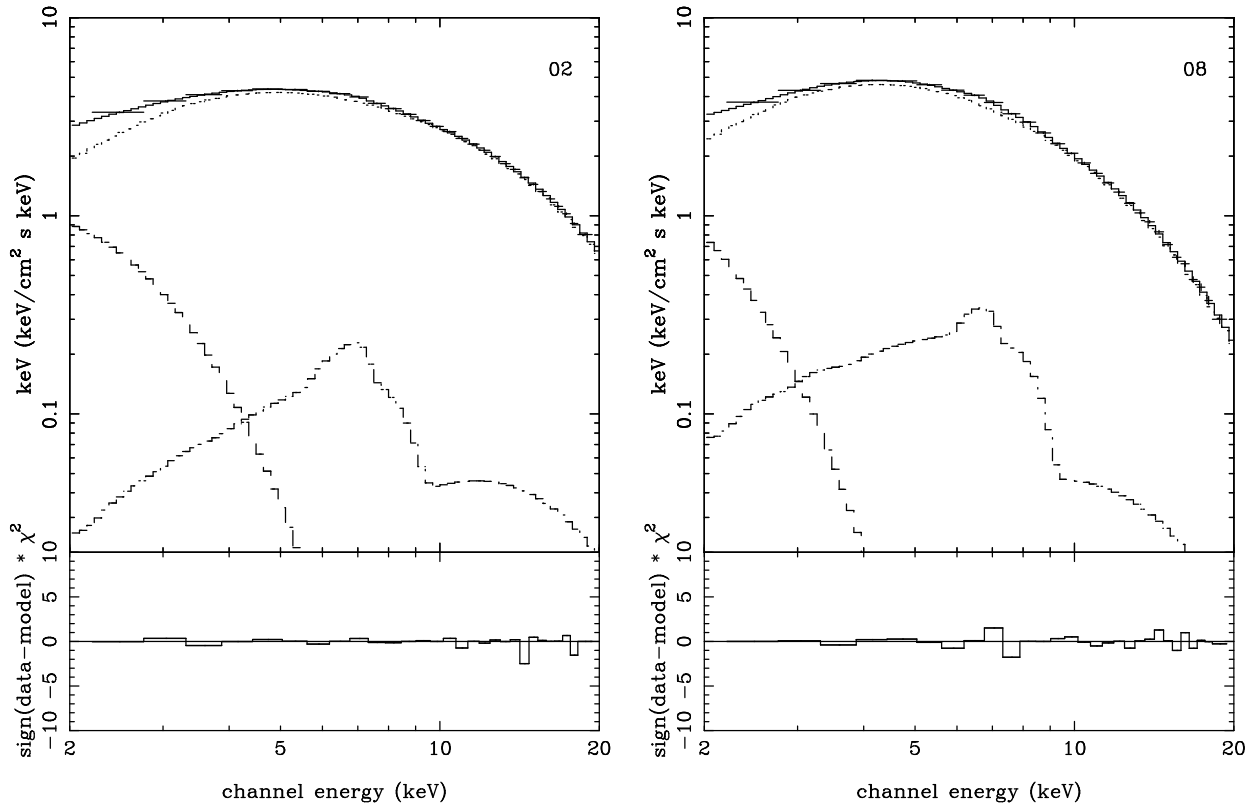


Figure 2. The two panels show spectral fits and residuals to 02 (horizontal branch: left hand panel) and 08 (flaring branch: right hand panel) spectra using the models detailed in Table 2. The low energy component shown by the dashed line is the disc blackbody, the dotted line is the comptonised continuum spectrum, the dashed-dotted line is its reflection from the disc while the solid line shows the total spectrum. The softening of the high energy emission is clearly the major difference between the horizontal and flaring branch spectra.

not contaminate the SUD count rate, unlike other X-ray binaries such as Cyg X-1. Finally, we note the the Galactic emission estimated from a couple of off-source regions near to Cyg X-2 is negligible.

The background subtracted data were rebinned on a 40 seconds timescale. The soft hardness (4.5–9.0 keV/1.1–4.5 keV) versus hard hardness (14.2–9.0 keV/4.5–9.0 keV) ratio for the June and October datasets are shown in Figure 1. These are identical to those presented by Hasinger et al., 1990. In the Hasinger et al., analysis, spectra were extracted at various intervals during the observations; to avoid spectral variations, these spectra were of short exposure. Here we extract spectra from each box in Figure 1, thus enabling us to obtain much longer exposures *but* avoiding any significant spectral variations and so a much more detailed analysis can be made. For the remainder of this paper, we refer to the spectra as 01–09, respectively.

5 SPECTRAL ANALYSIS

The interstellar column density to Cyg X-2 determined through visual extinction to the secondary star and the relative size of the X-ray dust scattering halo is $2.2 \times 10^{21} \text{ cm}^{-2}$ (Predehl & Schmitt 1995). This is consistent with the column seen from ROSAT, BBXRT, ASCA and SAX spectral analysis so we fix this in all the following fits.

Results from fitting models based on the ideas devel-

oped in Section 3 are given in Table 2. We obtain excellent fits to all the individual spectra (total $\chi^2_\nu = 136.8/180$) with optically thick disc emission and a Comptonised boundary layer together with its reflection from an ionized disc. The spectral fits for two different positions on the Z track (02 and 08) are shown in Figure 2.

Previous papers have often modelled the iron spectral features using a broad line. Table 3 shows the results obtained by replacing the more physically motivated reflected spectrum with an *ad hoc* broad iron line. The line energy and intrinsic width are constrained to be between 6.4–7 keV, and less than $\sigma \leq 0.42$ (corresponding to a $\text{FWHM} \leq 1 \text{ keV}$), respectively, for stability. The fit is adequate (although the model fails to describe the spectra on the normal branch - flaring branch transition) with $\chi^2_\nu = 211.9/180$. An F test shows that reflection is 99.98 per cent more probable to be the correct description of the spectral features than a broad Gaussian iron line.

Figure 3 shows how the derived continuum parameters evolve along the Z track using the best fitting reflection model for the spectral features (Table 2). All fluxes are derived by integrating the relevant unabsorbed model spectrum over 0.01–100 keV. The most significant change in the spectrum is the factor 2 increase in disc flux between spectra 4 and 5. However, despite this increase in accretion rate through the disc, the flux in the boundary layer stays constant to within 10 per cent, although its spectrum softens (seen both by an increase in spectral index and decrease in

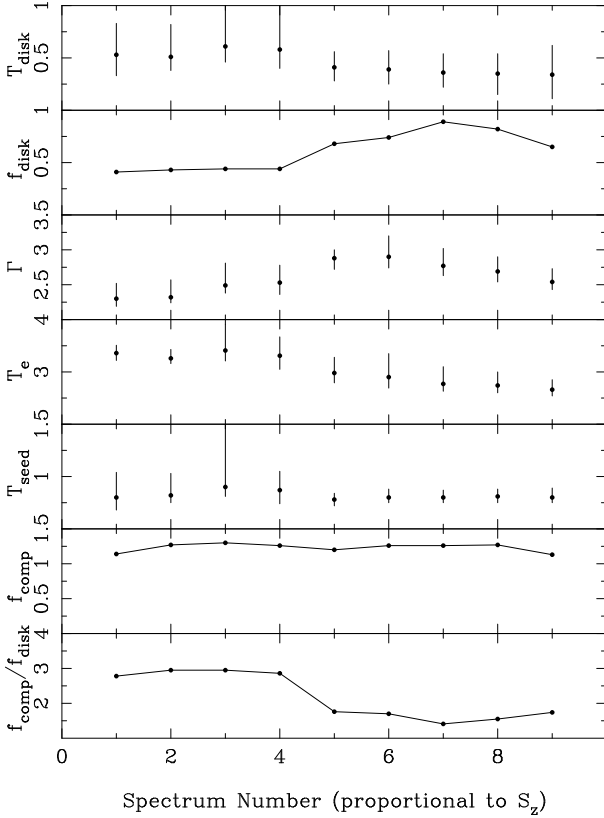


Figure 3. The derived continuum parameters for the spectral fits to the Eastern model with full boundary layer comptonization and reflection (`diskbb+thcomp+reflection`) given in Table 2 as a function of position along the Z track. All temperatures are given in keV, and all fluxes are in units of 10^{-8} ergs cm^{-2} s^{-1} . The only statistically significant changes are that the disc blackbody flux increases while the comptonised spectrum softens.

electron temperature). Thus the the ratio of flux dissipated in the boundary layer also makes an abrupt change between spectra 04 and 05, from ~ 3 to ~ 1.6 .

Figure 4 shows the evolution of the soft component in more detail. The disc temperature is clearly consistent with staying constant as the flux in the soft component increases (upper panel), which would imply that the optically thick boundary layer extends progressively over more and more of the inner disc, so the the observed inner disc radius increases. However, the uncertainties are large and cannot exclude the $T_{disc} \propto f_{disc}^{0.25}$ dependence expected for increasing accretion rate through a constant radius flow. The lower panel of figure 4 shows that the seed photons for the compton scattered component have a temperature which is again consistent with a constant but is significantly higher than the temperature of the observed soft component from the disc. This implies that the disc photons we observe are *not* the source of seed photons, and again, the most probable geometry is one where the optically thick comptonising cloud surrounds most of the neutron star surface and also perhaps the innermost disc.

The reflection parameters are shown in Figure 5. These are poorly determined since reflection is a curving spectral component and so is difficult to disentangle from the other two curving spectral components from the disc and comp-

tonised boundary layer. The spectral features help, but the relative contrast of these can be dramatically changed by ionization effects (and by relativistic smearing). All the parameters are consistent with a constant value ($\Omega/2\pi = 0.16$, $\xi = 330$ and $R_{in} = 120R_g$). However, the parameters are highly correlated, and *together* they are not consistent with these constant values. Fixing the reflected fraction (as appropriate if the geometry remains the same) at the mean value of $\Omega/2\pi = 0.16$ requires a significant change in the ionization parameter, as shown by the offset open symbols in Figure 5. Physically, what is happening is that the spectral features increase in intensity along the Z track, so either the solid angle subtended by the reflector increases or its ionization state increases. Since the solid angle here is fixed, then the ionization state increases. Alternatively of course, it could be that the ionization state remains fixed and the geometry changes or that both change. Unfortunately, the broadening of the spectral features is still largely unconstrained, these data cannot determine the inner disc radius from relativistic smearing.

6 ALTERNATIVE SPECTRAL MODELS

While this model gives a good description of the observed spectrum, the underlying continuum form is not unique. Even within the same physical picture of disc accretion and a comptonizing boundary layer there are different approaches to modelling the data. There are several approximate forms for the Comptonised spectrum. Our model, which is very similar to the `comp`tt model in XSPEC (Titarchuk 1994), includes the spectral curvature expected from having the seed photons within the observed bandpass. Previous papers have often used the `comp`st model (Sunyaev & Titarchuk 1980) or cutoff power law for the comptonised flux, but this is applicable *only* where the seed photons for the Comptonization are at much lower energies than the observed bandpass. This is plainly not the case for the Z sources (nor for *any* neutron star accreting at more than 0.1 per cent of Eddington).

In Table 4 we fit the phenomenological model of a disc blackbody, comptonised continuum without seed photons and broad iron line) to the data, and obtain very different results (compare to Table 3 where the comptonised model includes seed photon curvature). Firstly, the fits are much worse using the `comp`st approximation – typically by $\Delta\chi^2 \sim 10$ larger in each spectrum for one less model parameter (the seed photon energy). More importantly, the derived model parameters are very different. Figure 6 compares the continuum luminosities derived from the `comp`st model (Table 4), to those derived from the `thcomp` model (Table 3) where the curvature in the comptonised spectrum near the seed photon energy is included. The disc temperature is much higher in the `comp`st fits, as is its flux, but its implied radius is much smaller.

The mean radius of the inner disc derived from the `thcomp` approximation (including seed photon curvature) is 60_{-40}^{+13} km, compared with 9.2 ± 0.2 km from `comp`st (from the mean normalisation of the `diskbb` components, assuming that $\cos(\text{inclination})/D_{10}^2 \sim 1$ as appropriate for the best estimates of distance in units of 10 kpc, $D_{10} = 0.72$, and inclination of 60° : Orosz & Kuulkers 1999). Both are of order the neutron star radius, especially given the many

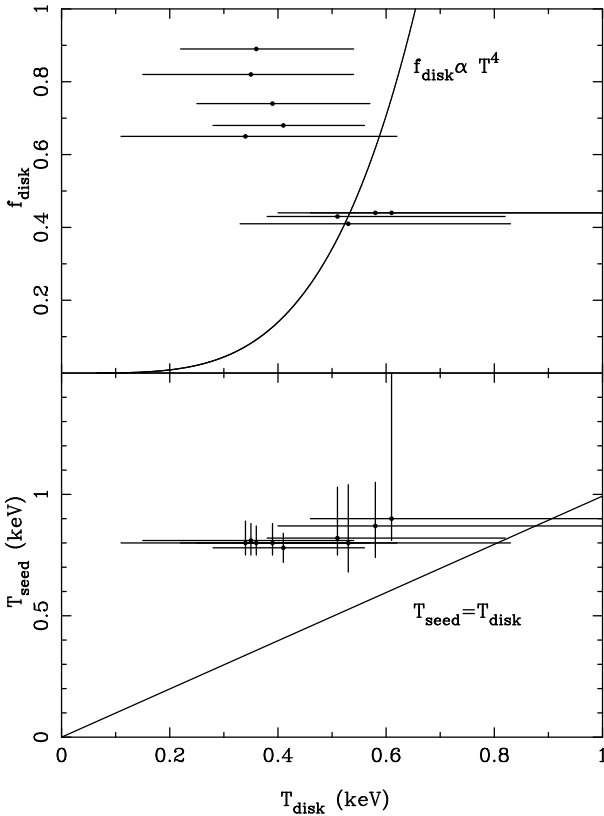


Figure 4. The soft spectral components from the Eastern model with full boundary layer comptonization and reflection (`diskbb+thcomp+reflection`). The upper panel shows disc temperature versus disc flux from the fits in table 2. The disc temperature is consistent with a constant as the flux varies by a factor 2, which would imply that the disc inner radius was increasing. However, the uncertainties are large and the data cannot rule out the expected flux–temperature dependence for a constant radius flow, shown by the solid curve. The lower panel shows the seed photon temperature as a function of the disc temperature. The seed photons are plainly significantly hotter than the observed disc temperature (the solid line shows $T_{seed} = T_{disc}$), showing that the observed soft component is not the major source of seed photons for the comptonizing cloud.

systematic effects inherent in the `diskbb` radius (neglect of colour temperature correction, relativistic effects and stress free inner boundary condition), but the apparent emitting area is suppressed by a factor of 7 by using an incorrect spectral form for the comptonised spectrum. Neglecting the turnover at the seed photon energy means that the contribution of the comptonised emission is overestimated at low energies, so the remaining flux to be associated with the disc emission is underestimated. Previous comparisons the Western and Eastern models have cited the very small emitting area of the disc as a problem for the Eastern models (e.g. Church & Balucinska–Church 2001), but here it is clear that the small area can be an artifact of incorrect spectral modelling of the comptonised component.

By contrast, changing the description of the disc emission does *not* dramatically change the inferred parameters for fluxes from the disc and boundary layer components. The `diskbb` disc blackbody model approximates the disc spectrum neglecting the stress-free inner boundary condition,

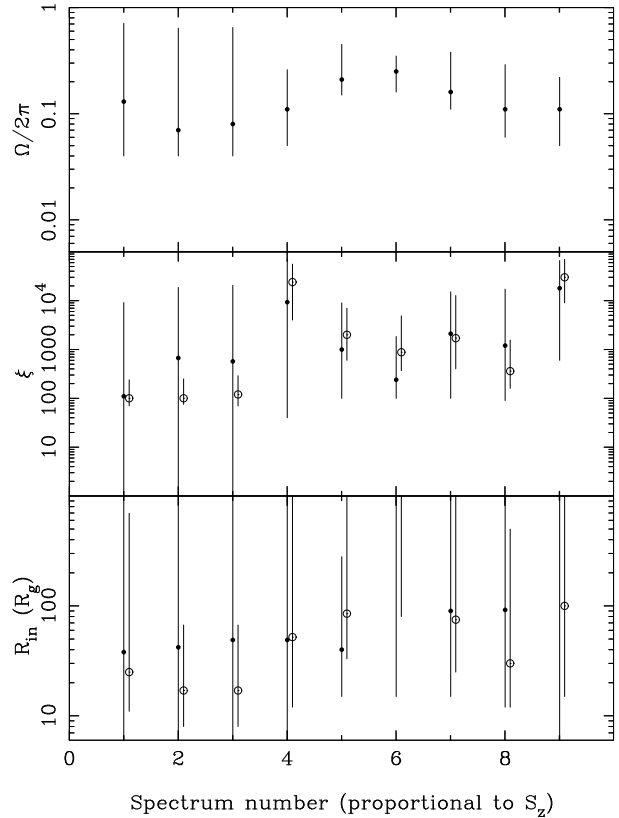


Figure 5. The derived reflected parameters from the Eastern model with full boundary layer comptonization and reflection (`diskbb+thcomp+reflection`) given in Table 2 as a function of position along the Z track. All the parameters are statistically consistent with constant values due to the large uncertainties, although this masks subtle spectral changes. Assuming that the solid angle subtended by the reflector is constant then there are significant changes in the ionization of the reflected spectrum. These are shown by the open symbols which are offset by 0.1 in spectral number.

relativistic corrections and any energy input from illumination, and assumes that the disc spectrum at any radius is a true blackbody (Mitsuda et al 1984). The `diskm` model in XSPEC (Stella & Rosner 1984) tackles two of these assumptions, in that it uses a modified blackbody spectrum to describe the disc spectrum where the opacity is dominated by electron scattering (Shakura & Sunyaev 1973), and includes the inner boundary condition. The spectrum is then somewhat broader than the `diskbb` model, but gives results which are more or less the same as those for the `diskbb` model in the 2–20 keV range in terms of the total disc flux, and concomitant comptonised continuum parameters. We fix the `diskm` spectrum normalisation = $\cos(\text{inclination})/D_{10}^2$ at unity (Orosz & Kuulkers 1999), alpha viscosity at 0.1 and mass of the neutron star at $1.4M_{\odot}$. Using the `diskm` model with the `thcomp` continuum and broad iron line to model the spectrum gives an adequate fit (total $\chi^2_{\nu} = 224.1/180$), but replacing the broad Gaussian line by the reflected spectrum again gives a significant improvement in the fit (total $\chi^2_{\nu} = 139.5/180$).

The differences between `diskm` and `diskbb` are quite subtle. However, if there is substantial comptonization of

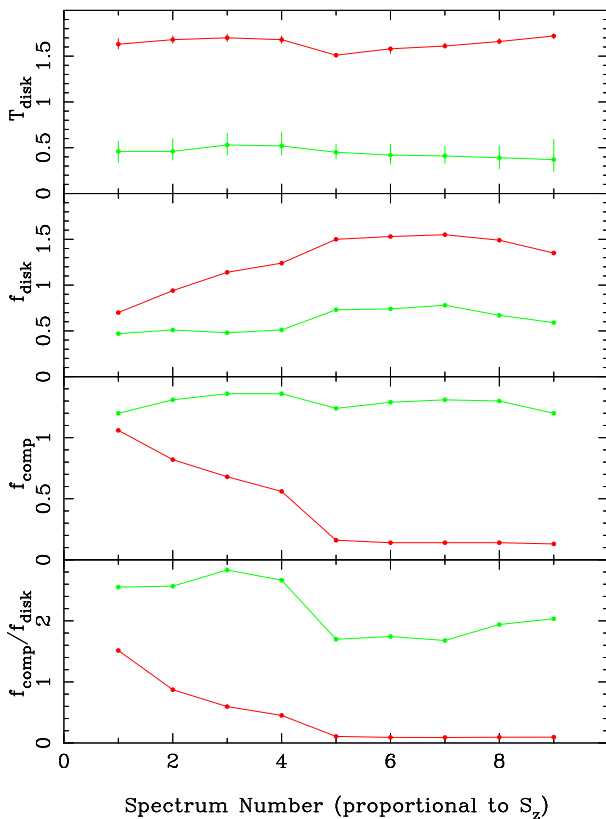


Figure 6. Continuum parameters derived from the Eastern model assuming approximate boundary layer comptonization (`compst`, dark grey, Table 4) compared to those derived from models which include the seed photon curvature (`thcomp`, light grey, Table 3). Both sets of fits have the disk spectrum modelled by `diskbb` and reflection is approximated by a gaussian line. The disc temperature is given in keV, and all fluxes are in units of 10^{-8} ergs cm^{-2} s^{-1} . Plainly there is a dramatic difference in the inferred continuum depending on whether the comptonised spectrum includes the effect of the seed photons. Given that the seed photon are expected to be within the observed bandpass then it is clear that approximations to the comptonised spectrum which do not include this can be severely misleading.

the disc emission then the disc spectrum can change dramatically. Such strong comptonization is sometimes seen in the Galactic Black Holes at high mass accretion rates (Życki, Done & Smith 2001). This is the basis of the ‘Western’ approach, in which it is the *disc* emission which is strongly comptonised, while the boundary layer is a (more or less) simple blackbody (White, Stella & Parmar 1988, see Section 2). Table 5 shows results from this with the commonly used `compst` model, together with the phenomenological broad iron line to model the spectral features. This is a good fit to the spectra (total $\chi^2_\nu = 171.5/189$), and has a blackbody boundary layer temperature of ~ 1 keV, but the ratio of the boundary layer to disc flux is much lower than that predicted for a non-rotating neutron star. This was noted by White et al., (1988) and suggested as evidence for equilibrium (fast!) neutron star spin periods. However, this result is *not* robust. The `compst` model assumes that the seed photons are far below the observed bandpass, so the spectrum is a power law below energies corresponding to the electron temperature. But the seed photons *must* be in the observed

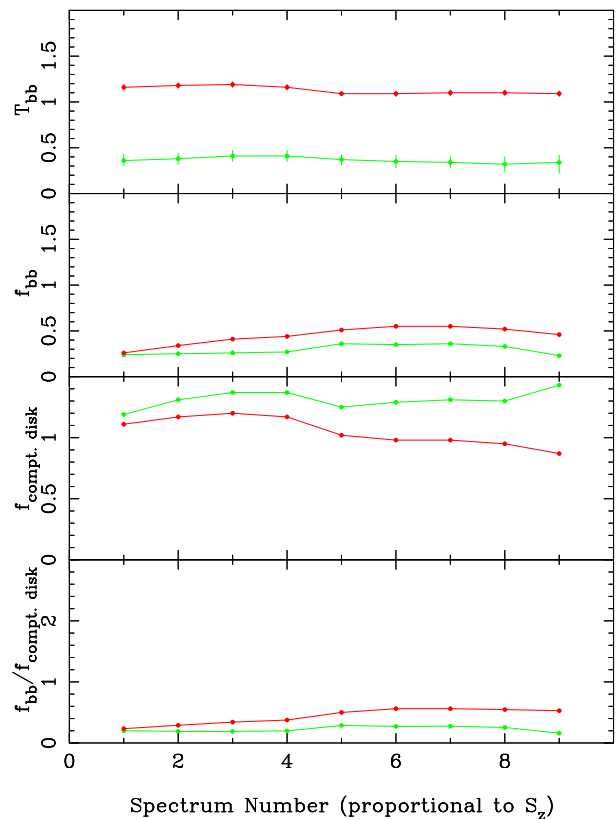


Figure 7. Continuum parameters derived from the Western model assuming approximate disc comptonization (`compst`, dark grey, Table 5) compared to those derived from models which include the seed photon curvature (`thcomp`, light grey, Table 6). Both sets of fits have the thermalized boundary layer modelled by `body` and reflection is approximated by a gaussian line. The approximate comptonisation model requires a blackbody at ~ 1 keV as appropriate for the boundary layer, but its luminosity is far below that of the disc. There is a substantial drop in the derived ‘boundary layer’ blackbody temperature to ~ 0.3 keV when the comptonised disc is modelled by the more physically realistic comptonization which includes the curvature expected at energies close to the seed photons. The blackbody temperature is given in keV, and all fluxes are in units of 10^{-8} ergs cm^{-2} s^{-1} .

energy range, since the assumption here is that it is the disc emission itself which is being comptonised. Using the `thcomp` model for the comptonised disc, so that the spectral curvature expected from the seed photons is included, gives very different results (Table 6). Figure 7 shows a comparison of the derived blackbody boundary layer temperature and flux for these two different disc comptonization models. Plainly the continuum parameters vary substantially, and again, we stress that using `compst` outside of the range where its approximations are valid can give misleading results.

Figure 8 compares the derived spectra for datasets 02 and 08 using the black body boundary layer plus comptonised disc approach. The upper panel shows the fits where the seed photon curvature is neglected, which is the standard approach in the literature, while the lower panel shows how the fits change when the seed photon curvature is included in the models. It is clear that the blackbody boundary layer temperature changes dramatically, from ~ 1 keV derived

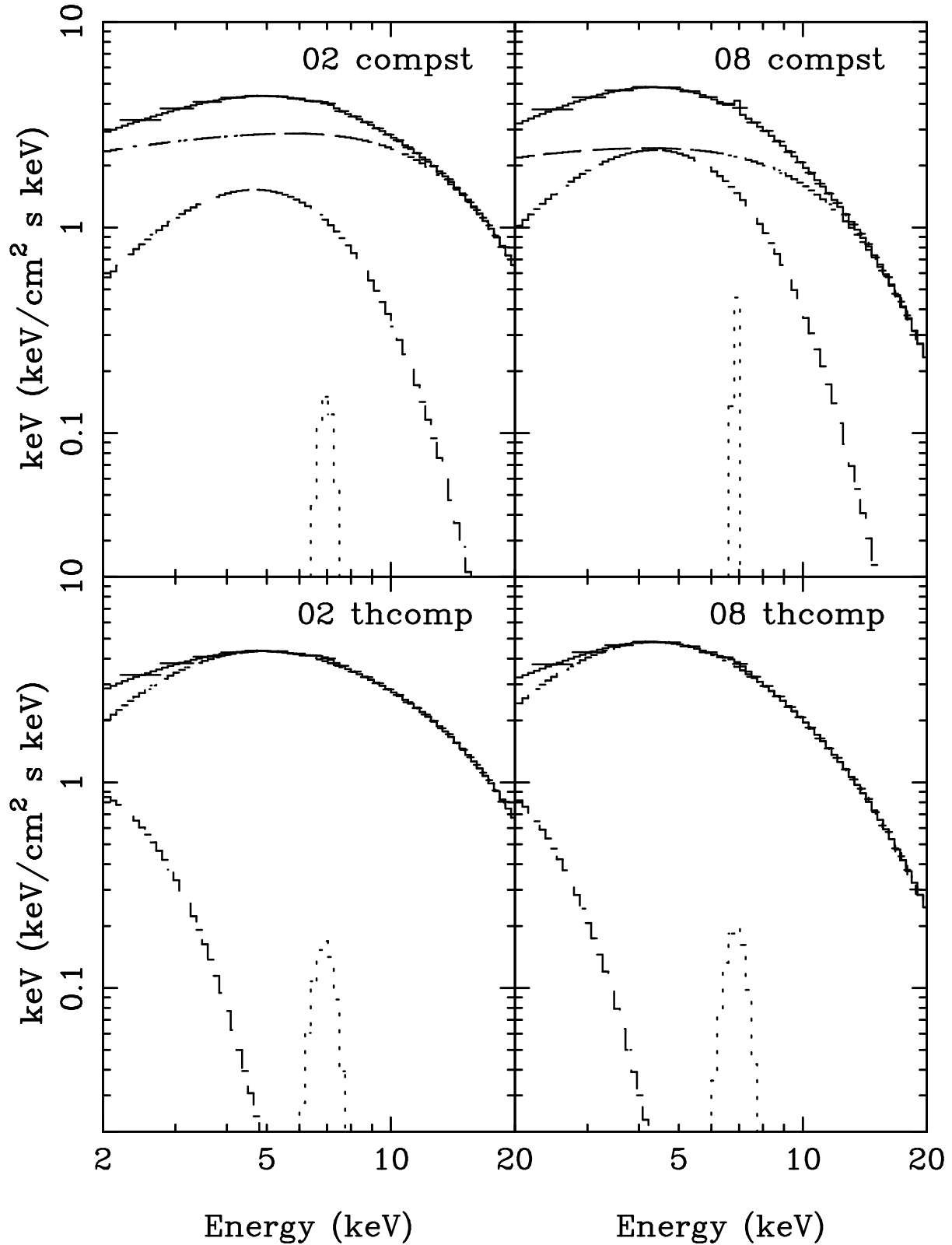


Figure 8. Spectra derived using the Western model, assuming that the disc emission is strongly comptonised while the boundary layer is mostly thermalised. The upper panel shows the derived fits to 02 (horizontal branch) and 08 (flaring branch) spectra using the `compst` model for the comptonised disc. This does not have the seed photon curvature included, and the data then require a high temperature ~ 1 keV blackbody component to fit the observed spectra. The lower panel shows the same data deconvolved using a model which does include the seed photon curvature in the comptonised spectrum. This dramatically changes the derived boundary layer temperature, reducing it to ~ 0.3 keV. Comptonization approximations which do not take into account the seed photons can give highly misleading results for the boundary layer emission.

Table 2. GINGA data fit to the Eastern model with comptonization of the boundary layer including seed photon curvature and full reflection (`diskbb + thcomp + reflection`)

data	kT_{diskbb} keV	f_{diskbb}^a	Γ	kT_e keV	kT_{seed} keV	f_{thcomp}^a	$\Omega/2\pi$	ξ	R_{in}	χ^2/ν
01	$0.53^{+0.30}_{-0.20}$	0.41	$2.30^{+0.22}_{-0.11}$	$3.36^{+0.15}_{-0.14}$	$0.80^{+0.24}_{-0.12}$	1.14	$0.13^{+0.58}_{-0.09}$	110^{+9000}_{-110}	$38^{+\infty}_{-32}$	8.4/20
02	$0.51^{+0.31}_{-0.13}$	0.43	$2.32^{+0.25}_{-0.08}$	$3.26^{+0.17}_{-0.10}$	$0.82^{+0.21}_{-0.07}$	1.27	$0.07^{+0.57}_{-0.03}$	670^{+18000}_{-670}	$42^{+\infty}_{-36}$	9.0/20
03	$0.61^{+0.90}_{-0.15}$	0.44	$2.49^{+0.32}_{-0.11}$	$3.41^{+0.50}_{-0.20}$	$0.90^{+1.22}_{-0.09}$	1.30	$0.08^{+0.57}_{-0.04}$	570^{+20000}_{-570}	$49^{+\infty}_{-43}$	12.0/20
04	$0.58^{+0.99}_{-0.18}$	0.44	$2.53^{+0.25}_{-0.17}$	$3.31^{+0.36}_{-0.26}$	$0.87^{+0.18}_{-0.13}$	1.26	$0.11^{+0.15}_{-0.06}$	9300^{+60000}_{-9260}	$49^{+\infty}_{-43}$	14.6/20
05	$0.41^{+0.15}_{-0.13}$	0.68	$2.88^{+0.12}_{-0.16}$	$2.98^{+0.30}_{-0.19}$	0.78 ± 0.06	1.20	$0.21^{+0.24}_{-0.06}$	1000^{+8000}_{-900}	40^{+240}_{-25}	24.8/20
06	$0.39^{+0.18}_{-0.14}$	0.74	$2.90^{+0.30}_{-0.16}$	$2.90^{+0.45}_{-0.21}$	$0.80^{+0.08}_{-0.05}$	1.26	$0.25^{+0.10}_{-0.09}$	240^{+1600}_{-140}	$1000^{+\infty}_{-985}$	15.6/20
07	$0.36^{+0.18}_{-0.14}$	0.89	$2.77^{+0.25}_{-0.14}$	$2.77^{+0.33}_{-0.14}$	$0.80^{+0.07}_{-0.05}$	1.26	$0.16^{+0.22}_{-0.05}$	2100^{+13000}_{-2000}	$90^{+\infty}_{-75}$	22.6/20
08	$0.35^{+0.19}_{-0.20}$	0.82	$2.69^{+0.21}_{-0.15}$	$2.74^{+0.26}_{-0.14}$	$0.81^{+0.07}_{-0.06}$	1.28	$0.11^{+0.18}_{-0.05}$	1200^{+16000}_{-1110}	$92^{+\infty}_{-80}$	12.4/20
09	$0.34^{+0.28}_{-0.23}$	0.64	$2.54^{+0.19}_{-0.11}$	$2.66^{+0.19}_{-0.12}$	$0.80^{+0.09}_{-0.05}$	1.13	$0.11^{+0.11}_{-0.06}$	$1.80^{+4.8}_{-1.74} \times 10^4$	$1000^{+\infty}_{-994}$	17.4/20

^a all fluxes are the unabsorbed model, integrated from 0.01–100 keV, in units of 10^{-8} ergs $\text{s}^{-1} \text{cm}^{-2}$

Table 3. GINGA data fit to the Eastern model with comptonization of the boundary layer including seed photon curvature with approximate reflection (`diskbb + thcomp + gau`)

data	kT_{diskbb} keV	f_{diskbb}^a	Γ	kT_e keV	kT_{seed} keV	f_{thcomp}^a	E_{line} keV ^b	σ keV ^c	EW (eV)	χ^2/ν
01	$0.46^{+0.11}_{-0.12}$	0.47	2.30 ± 0.05	$3.42^{+0.11}_{-0.10}$	$0.78^{+0.06}_{-0.05}$	1.20	6.7 ± 0.3	$0.42_{-0.41}$	50 ± 18	11.0/20
02	$0.46^{+0.14}_{-0.09}$	0.51	$2.35^{+0.06}_{-0.04}$	$3.34^{+0.11}_{-0.07}$	$0.83^{+0.05}_{-0.04}$	1.31	6.8 ± 0.2	$0.42_{-0.42}$	52^{+11}_{-22}	12.5/20
03	$0.53^{+0.13}_{-0.11}$	0.48	$2.53^{+0.08}_{-0.07}$	$3.50^{+0.17}_{-0.13}$	$0.88^{+0.07}_{-0.05}$	1.36	$6.9^{+0.1}_{-0.3}$	$0.42_{-0.42}$	50^{+17}_{-20}	15.1/20
04	$0.52^{+0.15}_{-0.10}$	0.51	$2.67^{+0.12}_{-0.10}$	$3.58^{+0.30}_{-0.19}$	$0.89^{+0.07}_{-0.05}$	1.36	$7.0_{-0.2}$	$0.42_{-0.27}$	52^{+18}_{-19}	20.2/20
05	$0.45^{+0.09}_{-0.07}$	0.73	$3.30^{+0.20}_{-0.14}$	$3.77^{+0.62}_{-0.34}$	$0.86^{+0.05}_{-0.03}$	1.24	$6.8^{+0.1}_{-0.2}$	$0.42_{-0.08}$	97 ± 20	47.7/20
06	$0.42^{+0.12}_{-0.10}$	0.74	$3.24^{+0.25}_{-0.20}$	$3.53^{+0.70}_{-0.43}$	$0.87^{+0.05}_{-0.04}$	1.29	6.7 ± 0.2	$0.42_{-0.10}$	100^{+26}_{-23}	29.5/20
07	$0.41^{+0.11}_{-0.08}$	0.78	$3.15^{+0.22}_{-0.14}$	$3.32^{+0.50}_{-0.34}$	$0.87^{+0.05}_{-0.03}$	1.31	6.8 ± 0.2	$0.42_{-0.14}$	$86^{+0.20}_{-25}$	38.8/20
08	$0.39^{+0.13}_{-0.12}$	0.67	$2.89^{+0.17}_{-0.12}$	$3.00^{+0.27}_{-0.18}$	$0.86^{+0.05}_{-0.04}$	1.30	6.8 ± 0.2	$0.42_{-0.42}$	60^{+15}_{-25}	15.8/20
09	$0.37^{+0.22}_{-0.13}$	0.59	$2.72^{+0.17}_{-0.09}$	$2.83^{+0.22}_{-0.12}$	$0.85^{+0.06}_{-0.04}$	1.20	$7.0_{-0.2}$	$0.42_{-0.42}$	50^{+16}_{-23}	21.3/20

^a all fluxes are the unabsorbed model, integrated from 0.01–100 keV, in units of 10^{-8} ergs $\text{s}^{-1} \text{cm}^{-2}$

^b Energy constrained to be between 6.4–7 keV

^c Width constrained to be between 0–0.42 keV

from the inapplicable `compst` model to ~ 0.3 keV, in models with the seed photon compton curvature (`thcomp`).

7 DISCUSSION AND CONCLUSIONS

The spectrum of Cyg X-2 has complex curvature which makes spectral fitting highly non-unique. It is generally agreed that the X-ray spectrum must consist of at least two components, the disc and the boundary layer, and that at least one of these (though more probably both) is comptonised. In addition, there are spectral features corresponding to ionised iron K, which are often modelled as a broad Gaussian line. We have shown that the derived spectral parameters are crucially dependent on how the comptonised spectrum is modelled. The often used `compst` or cutoff power law models are physically inconsistent since the seed photons for the compton scattering *must* be in the observed X-ray range, whether they come from the disc or the boundary layer. The lack of curvature in `compst` or cutoff power laws at energies below the electron temperature then forces a blackbody at ~ 1 keV into the fit. This is purely an artifact of incorrect modelling of the comptonised spectrum and has

no physical relation to the boundary layer or neutron star surface.

When the comptonised spectrum is modelled including this curvature (using `thcomp` or `compst`) then the spectrum is adequately fit either by assuming that the boundary layer is comptonised, and the softer emission is from the accretion disc (`diskbb+thcomp+gau` $\chi^2_\nu = 211.9/180$) or that the disc spectrum is comptonised, and the boundary layer is a blackbody (`bb+thcomp+gau` $\chi^2_\nu = 207.3/180$). The GINGA data cannot distinguish between these models statistically. However, there are some theoretical constraints on the ratio of the disc and boundary layer fluxes. In the ‘Eastern model’, where the boundary layer is comptonised, we derive a boundary layer luminosity which is about twice that of the luminosity of the disc. This is as expected in the general relativistic models of the gravitational potential if the neutron star spin is not close to the Keplerian breakup frequency (Sunyaev & Shakura 1986). By contrast, in the ‘Western model’ where the disc is strongly comptonised, the ratio of the boundary layer blackbody luminosity to that from the disc is $\sim 0.2 - 0.25$, implying that the neutron star is significantly spun up. Detailed calculations indicate that to get a ratio of boundary layer to disc flux this low requires that the spin frequency of the neutron star is ≥ 1 kHz (Sibgatullin &

Table 4. GINGA data fit to the Eastern model with approximate comptonization of the boundary layer and approximate reflection (`diskbb + compst + gaussian`)

data	kT_{diskbb} keV	f_{diskbb}^a	kT_e (keV)	τ_e	f_{compst}^a	E_{line} keV ^b	σ keV ^c	EW (eV)	χ^2/ν
01	$1.63^{+0.06}_{-0.05}$	0.70	2.93 ± 0.07	$14.5^{+1.4}_{-1.0}$	1.06	6.7 ± 0.2	$0.42_{-0.42}$	50^{+15}_{-20}	10.4/21
02	1.68 ± 0.04	0.94	$2.86^{+0.08}_{-0.05}$	$16.6^{+3.5}_{-1.5}$	0.82	$6.7^{+0.3}_{-0.2}$	$0.42_{-0.42}$	47^{+15}_{-14}	13.0/21
03	1.70 ± 0.04	1.14	$2.87^{+0.10}_{-0.11}$	$17.4^{+5.7}_{-2.1}$	0.68	$6.8^{+0.2}_{-0.3}$	$0.42_{-0.42}$	48^{+13}_{-14}	16.9/21
04	1.68 ± 0.04	1.24	$2.82^{+0.14}_{-0.17}$	$18.3^{+\infty}_{-3.0}$	0.56	$6.9^{+0.1}_{-0.2}$	$0.42_{-0.28}$	53^{+18}_{-17}	21.9/21
05	1.51 ± 0.02	1.50	$2.44^{+0.22}_{-0.05}$	$200^{+\infty}_{-185}$	0.16	$6.7^{+0.1}_{-0.2}$	$0.42_{-0.06}$	105 ± 20	50.6/21
06	$1.58^{+0.02}_{-0.05}$	1.53	$2.55^{+0.11}_{-0.10}$	$200^{+\infty}_{-180}$	0.14	$6.5^{+0.2}_{-0.1}$	$0.42_{-0.10}$	95 ± 20	41.0/21
07	$1.61^{+0.03}_{-0.02}$	1.55	$2.58^{+0.10}_{-0.09}$	$200^{+\infty}_{-177}$	0.14	6.6 ± 0.2	$0.42_{-0.14}$	73^{+17}_{-12}	59.7/21
08	$1.66^{+0.03}_{-0.02}$	1.49	2.59 ± 0.09	$200^{+\infty}_{-175}$	0.14	$6.5^{+0.4}_{-0.1}$	$0.42_{-0.42}$	50^{+18}_{-20}	47.6/21
09	$1.72^{+0.02}_{-0.03}$	1.35	$2.63^{+0.10}_{-0.08}$	$200^{+\infty}_{-175}$	0.13	6.7 ± 0.3	$0^{+0.42}$	22^{+14}_{-12}	60.8/21

^a all fluxes are the unabsorbed model, integrated from 0.01–100 keV, in units of 10^{-8} ergs s⁻¹ cm⁻²^b Energy constrained to be between 6.4–7 keV^c Width constrained to be between 0–0.42 keV**Table 5.** GINGA data fit to the Western model with approximate comptonization of the disc and approximate reflection (`bbody + compst + gau`).

data	kT_{bb} (keV)	f_{bb}^a	kT_e (keV)	τ	f_{compst}^a	E_{line} keV ^b	σ keV ^c	EW (eV)	χ^2/ν
01	1.16 ± 0.03	0.26	2.95 ± 0.05	12.0 ± 0.3	1.86	6.8 ± 0.2	0.2 ± 0.2	35 ± 17	7.5/21
02	1.18 ± 0.03	0.34	2.87 ± 0.04	12.4 ± 0.3	1.92	$6.9^{+0.1}_{-0.3}$	$0.3^{+0.1}_{-0.3}$	30^{+20}_{-16}	9.7/21
03	1.19 ± 0.03	0.41	$2.84^{+0.06}_{-0.04}$	12.2 ± 0.3	2.02	$7.0_{-0.3}$	$0.4_{-0.4}$	34 ± 20	17.0/21
04	1.16 ± 0.03	0.44	$2.78^{+0.08}_{-0.06}$	12.1 ± 0.4	2.06	$7.0_{-0.2}$	$0.4_{-0.2}$	44^{+16}_{-22}	19.4/21
05	1.09 ± 0.02	0.51	2.55 ± 0.07	11.1 ± 0.4	2.45	6.8 ± 0.1	$0.4_{-0.1}$	80^{+20}_{-10}	32.2/21
06	1.09 ± 0.03	0.55	2.46 ± 0.10	11.9 ± 0.6	2.12	6.7 ± 0.2	$0.4_{-0.1}$	90 ± 25	21.2/21
07	1.10 ± 0.03	0.55	2.44 ± 0.08	12.2 ± 0.6	2.01	$6.9^{+0.1}_{-0.2}$	$0.4_{-0.2}$	70 ± 20	30.9/21
08	1.10 ± 0.03	0.52	2.38 ± 0.06	13.1 ± 0.6	1.73	6.8 ± 0.2	$0^{+0.4}$	38^{+30}_{-16}	11.9/21
09	1.09 ± 0.03	0.46	2.34 ± 0.05	14.0 ± 0.6	1.44	$7.0_{-0.2}$	$0.4_{-0.4}$	38^{+18}_{-23}	21.7/21

^a all fluxes are the unabsorbed model, integrated from 0.01–100 keV, in units of 10^{-8} ergs s⁻¹ cm⁻²^b Energy constrained to be between 6.4–7 keV^c Width constrained to be between 0–0.42 keV**Table 6.** GINGA data fit to the Western model with full comptonization of the disc and approximate reflection (`bbody + thcomp + gau`).

data	kT_{bb} (keV)	f_{bb}^a	Γ (keV)	kT_e	kT_{seed}	f_{thcomp}^a	E_{line} keV ^b	σ keV ^c	EW (eV)	χ^2/ν
01	$0.36^{+0.07}_{-0.06}$	0.24	$2.29^{+0.05}_{-0.04}$	$3.42^{+0.10}_{-0.09}$	0.78 ± 0.05	1.19	6.8 ± 0.2	$0.42_{-0.42}$	50^{+18}_{-20}	10.5/20
02	0.38 ± 0.06	0.25	2.36 ± 0.05	$3.35^{+0.10}_{-0.08}$	0.83 ± 0.04	1.31	6.8 ± 0.2	$0.42_{-0.42}$	50^{+12}_{-20}	11.9/20
03	0.41 ± 0.06	0.26	2.52 ± 0.07	$3.49^{+0.17}_{-0.12}$	0.88 ± 0.04	1.37	$6.9^{+0.1}_{-0.2}$	$0.42_{-0.42}$	48^{+18}_{-20}	14.4/20
04	0.41 ± 0.06	0.27	2.67 ± 0.10	$3.57^{+0.28}_{-0.20}$	0.89 ± 0.04	1.37	$7.0_{-0.2}$	$0.42_{-0.42}$	51^{+18}_{-20}	19.5/20
05	0.37 ± 0.05	0.36	$3.31^{+0.18}_{-0.14}$	$3.79^{+0.61}_{-0.34}$	0.86 ± 0.03	1.25	$6.8^{+0.1}_{-0.2}$	$0.42_{-0.10}$	95 ± 20	46.7 /20
06	0.35 ± 0.07	0.35	$3.25^{+0.23}_{-0.20}$	$3.54^{+0.69}_{-0.42}$	0.87 ± 0.04	1.29	6.7 ± 0.2	$0.42_{-0.10}$	100 ± 25	29.1/20
07	0.34 ± 0.06	0.36	$3.15^{+0.21}_{-0.13}$	$3.32^{+0.47}_{-0.16}$	0.87 ± 0.04	1.31	$6.8^{+0.2}_{-0.1}$	$0.42_{-0.14}$	85^{+10}_{-25}	38.3/20
08	0.32 ± 0.08	0.33	$2.89^{+0.16}_{-0.10}$	$2.99^{+0.25}_{-0.14}$	0.86 ± 0.04	1.30	6.8 ± 0.2	$0.42_{-0.42}$	64^{+16}_{-30}	15.7/20
09	$0.34^{+0.08}_{-0.12}$	0.23	$2.74^{+0.13}_{-0.11}$	$2.86^{+0.16}_{-0.15}$	0.86 ± 0.04	1.43	$7.0_{-0.2}$	$0.42_{-0.42}$	45 ± 21	21.2/20

^a all fluxes are the unabsorbed model, integrated from 0.01–100 keV, in units of 10^{-8} ergs s⁻¹ cm⁻²^b Energy constrained to be between 6.4–7 keV^c Width constrained to be between 0–0.42 keV

Sunyaev 2000). This seems excessive: all known millisecond pulsars (the descendants of the LMXB neutron stars) have spin frequencies ≤ 700 Hz (e.g. Kramer et al., 1998).

Thus it seems likely that the ‘Eastern’ model (Mitsuda et al., 1984; 1989) is correct and that the boundary layer dominates the hard spectrum, while the disc dominates at softer energies. A standard objection to this approach, that in general the derived disc parameters require an emitting area which is far too small to be a true disc (e.g. Church & Balucinska-Church 2001), is again purely an artifact of incorrect modelling of the curvature due to the seed photons in the comptonised continuum.

Finally, it is clear that the residual spectral features at iron are considerably better described by a strongly ionised reflected spectrum than by a broad Gaussian line.

REFERENCES

- Asai K., Dotani T., Nagase F., Mitsuda K., 2000, *ApJS*, 131, 571
 Barret D., Olive J.F., Boirin L., Done C., Skinner G.K., Grindley J.E., 2000, *ApJ*, 533, 329
 Bautista M. A., Kallman T. R., Angelini L., Liedahl D. A., Smits D. P., 1998, *ApJ*, 509, 848
 Begelman M. C., McKee C. F., Shields G. A., 1983, *ApJ*, 271, 70
 Brandt W. N., Matt G., 1994, *MNRAS*, 268, 1051
 Church M. J., Balucinska-Church M., 2001, *A&A*, 369, 915
 Czerny M., Czerny B., Grindlay J. E., 1986, *ApJ* 311, 241
 Done C., Życki P. T., 1999, *MNRAS*, 305, 457
 di Salvo T., Robba N. R., Iaria R., Stella L., Burderi L., Israel G. L., 2001, *ApJ*, 554, 49
 di Salvo T., et al., 2000, *ApJ*, 544, L119
 Ebisawa K., Mitsuda K., Hanawa T., 1991, *ApJ*, 367, 213
 Fabian A. C., Rees M. J., Stella L., White N. E., 1989, *MNRAS*, 238, 729
 Fabian A. C., Iwasawa K., Reynolds C. S., Young A. J., 2000, *PASP*, 112, 1145
 Guainazzi M., Parmar A. N., Segreto A., Stella L., dal Fiume D., Oosterbroek T., 1998, *A&A*, 339, 802
 Hasinger G., Van der Klis M., 1989, *A&A*, 225, 79
 Hasinger G., van der Klis M., Ebisawa K., Dotani T., Mitsuda K., 1990, *A&A*, 235, 131
 Hayashida K., Inoue H., Koyama K., Awaki H., Takano S., 1989, *PASJ*, 41, 345
 Hirano T., Hayakawa S., Nagase F., Masai K., Mitsuda K., 1987, *PASJ*, 39, 619
 Hua X., Titarchuk L., 1995, *ApJ*, 449, 188
 Inogamov N. A., Sunyaev R. A., 1999, *AstL*, 25, 269
 in’t Zand J. J. M., Heise J., Kuulkers E., Bazzano A., Cocchi M., Ubertini P., 1999, *A&A*, 347, 891
 Kallman T. R., White N. E., 1989, *ApJ*, 341, 955
 Kallman T. R., 1995, *ApJ*, 455, 603
 Ko Y.-K., Kallman T. R., 1994, *ApJ*, 431, 273
 Kramer M., et al., 1998, *ApJ*, 501, 270
 Kuulkers E., Parmar A. N., Owens A., Oosterbroek T., Lammers U., 1997, *A&A*, 323, L29
 Lamb, F. K., 1989, in *Proc. 23rd ESLAB Symp. on Two Topics in X-Ray Astronomy*, ed. N. E. White (ESA SP-296) (Paris: ESA), p215
 Merloni A., Fabian A. C., Ross R. R., 2000, *MNRAS*, 313, 193
 Miller K. A., Stone J. M., 1997, *ApJ*, 489, 890
 Mitsuda K., et al., 1984, *PASJ*, 36, 741
 Mitsuda K., Inoue H., Nakamura N., Tanaka Y., 1989, *PASJ*, 41, 97
 Morrison R., McCammon D., 1983, *ApJ*, 270, 119
 Orosz J. A., Kuulkers E., 1999, *MNRAS*, 305, 132
 Piraino S., Santangelo A., Ford E. C., Kaaret P., 1999, *A&A* 349, L77
 Popham R., Sunyaev R.A., 2001, *ApJ*, 547, 355
 Predehl P., Schmitt J.H.M.M., *A&A*, 1995, 293, 889
 Psaltis D., Lamb F. K., Miller G. S., 1995, *ApJ*, 454, L137
 Raymond J. C., 1993, *ApJ*, 412, 267
 Sibgatullin N. R., Sunyaev R. A., 2000, *Astr. Letts.*, 26, 699
 Shakura N. I., Sunyaev R. A., 1973, *A&A*, 24, 337
 Shimura T., Takahara F., 1995, *ApJ*, 445, 780
 Smale A. P., et al., 1993, *ApJ*, 410, 796
 Stella L., Rosner R., 1984, *ApJ*, 277, 312
 Sunyaev R. A., Titarchuk L., 1980, *A&A*, 86, 121
 Sunyaev R. A., Shakura N. I., 1986, *Sov. Astr. Letts.*, 12, 117
 Tanaka Y., 1995, *Nature*, 375, 659
 Titarchuk L., 1994, *ApJ*, 434, 570
 Van der Klis M., 1995, in Lewin W. H. G., van Paradijs J., van den Heuvel E. P. J., eds., *X-ray Binaries*, Cambridge University Press, Cambridge, p252
 van Paradijs J., van der Klis M., 1994, *A&A*, 281, L17
 Vrtilik S. A., Soker N., Raymond J. C., 1993, *ApJ*, 404, 696
 Wardzinski G., Zdziarski A. A., 2000, *MNRAS*, 314, 183
 White N. E., Stella L., Parmar A. N., 1988, *ApJ*, 324, 363
 White N. E., Nagase F., & Parmar A. N., 1995, in Lewin W. H. G., van Paradijs J., van den Heuvel E. P. J., eds., *X-ray Binaries*, Cambridge University Press, Cambridge, p1
 White N. E., Peacock A., Taylor B. G., 1985, *ApJ*, 296, 475
 Williams O. R., et al., 1992, *ApJ*, 389, 157
 Yoshida K., Mitsuda K., Ebisawa K., Ueda Y., Fujimoto R., Yaqoob T., Done C., 1993, *PASJ*, 45, 605.
 Zdziarski A. A., Johnson W. N., Magdziarz P., 1996, *MNRAS*, 283, 193
 Życki P. T., Done C., Smith D. A., 1997, *ApJ*, 448, L113.
 Życki P. T., Done C., Smith D. A., 1998, *ApJ*, 496, L25.
 Życki P. T., Done C., Smith D. A., 1999, *MNRAS*, 305, 231
 Życki P. T., Done C., Smith D. A., 2001, *MNRAS*, in press